

This item is the archived peer-reviewed author-version of:

Evolution of multi-annual and large-scale phytoplankton patterns in the Scheldt estuary : the disappearance of phytoplankton accumulation in the brackish region

Reference:

Horemans Dante, Dijkstra Yoeri M., Tackx Michele, Meire Patrick, Cox Tom.- Evolution of multi-annual and large-scale phytoplankton patterns in the Scheldt estuary : the disappearance of phytoplankton accumulation in the brackish region
Estuarine, coastal and shelf science - ISSN 1096-0015 - 282(2023), 108258
Full text (Publisher's DOI): <https://doi.org/10.1016/J.ECSS.2023.108258>
To cite this reference: <https://hdl.handle.net/10067/1978280151162165141>

Evolution of multi-annual and large-scale phytoplankton patterns in the Scheldt estuary: the disappearance of phytoplankton accumulation in the brackish region

Dante M. L. Horemans^a, Yoeri M. Dijkstra^b, Michèle Tackx^c, Patrick Meire^a and Tom J. S. Cox^a

^aEcosystem Management Research Group, University of Antwerp, Universiteitsplein 1 C, Wilrijk, 2610, Antwerpen, Belgium

^bDelft Institute of Applied Mathematics, Delft University of Technology, Van Mourik Broekmanweg 6, Delft, 2822 XE, Zuid-Holland, Netherlands

^cLaboratoire Ecologie Fonctionnelle et Environnement, Université de Toulouse, CNRS, Toulouse INP, Université Toulouse 3 - Paul Sabatier (UPS), Route de Narbonne 118, Toulouse, 31062, Haute-Garonne, France

ARTICLE INFO

Keywords:

Phytoplankton
Zooplankton
iFlow model
Scheldt estuary
Light limitation
Equifinality


ABSTRACT

Estuaries often show regions in which Chlorophyll-a (Chl-a) accumulates. The location and magnitude corresponding to such accumulation result from a complex interplay between processes such as river flushing, salinity, nutrients, grazing on phytoplankton, and the light climate in the water column. An example is the multi-annual evolution of the estuary-scale Chl-a distribution in the Scheldt estuary (Belgium/Netherlands) in spring. From 2004-2007, we observed a limited spring bloom in the brackish region (km 60-90 from the mouth, salinity ~ 1-10 ppt). This bloom intensified in 2008-2014 and disappeared after 2015. This multi-annual evolution of Chl-a has been hypothesized to be linked to simultaneous multi-annual trends in the suspended particulate matter (SPM) distribution in summer and winter between 1995-2015 and the improvement of the water quality (e.g., reduction of ammonium), which affects grazing on phytoplankton by zooplankton. However, this hypothesis has not been systematically investigated. In this contribution, we apply a modeling approach in which observations are the core. We first analyze multi-annual in situ observations covering the full estuary. These observations include the SPM concentration, zooplankton abundance, and other variables affecting the Chl-a concentration. They show a multi-annual estuary-scale evolution not only in the SPM distribution but also in zooplankton abundance, freshwater discharge, and phytoplankton photosynthetic characteristics. Next, we apply a model approach that consists of an extensive sensitivity study and four model scenarios that are supported by these observations to constrain the processes and corresponding parameter variability that may have caused the observed change in Chl-a. Our results suggest that a change in SPM alone cannot explain the Chl-a observations. Instead, a multi-annual change in mortality rate, which we can attribute to both grazing by zooplankton and phytoplankton community (i.e., mortality dependence on salinity), may explain the multi-annual estuary-scale evolution of Chl-a in spring. Different model parameter choices may thus lead to similar model results (equifinality). Our results highlight that insight into the zooplankton dynamics and phytoplankton community characteristics is essential to understand the phytoplankton (cf. Chl-a) dynamics in the Scheldt estuary and that additional data regarding mortality and grazing rates is required to further constrain the model parameters.

1. Introduction

Estuaries regularly exhibit zones with locally elevated Chlorophyll-a (Chl-a) concentrations, which result from a complex interaction between physical, transport-related processes and chemical-biotic factors that determine net local phytoplankton growth. Such processes are governed by water temperature variations (Eppley, 1972), river flushing (Filardo and Dunstan, 1985; Liu and de Swart, 2015), salinity variations (Lucas et al., 1998), grazing on phytoplankton (Alpine and Cloern, 1992; Lionard et al., 2005), nutrient dynamics (Tilman et al., 1982; Cira et al., 2016), and the light climate in the water column (Sverdrup, 1953; Desmit et al., 2005).

Human influences may cause gradual (i.e., multi-annual) changes in multiple of these interacting processes. Examples are the multi-annual changes in suspended particulate matter (SPM) dynamics caused by channel deepening

 DMLHoremans@pm.me (D.M.L. Horemans)

ORCID(s): 0000-0003-0106-8122 (D.M.L. Horemans); 0000-0003-0682-0969 (Y.M. Dijkstra); 0000-0001-6832-6865 (M. Tackx); 0000-0003-2599-5350 (P. Meire); 0000-0002-7280-8047 (T.J.S. Cox)

51 in the Ems estuary (Winterwerp et al., 2013; Dijkstra et al., 2019c) and the multi-annual evolution in nutrients in the
52 Scheldt estuary resulting from an increase in wastewater treatment capacity (Brion et al., 2015). Modeling the exact
53 mechanisms that may have caused the observed changes in phytoplankton dynamics is challenging due to the high
54 complexity and because many of the biological interactions are poorly constrained by available data, especially when
55 considering multi-annual time scales.

56 In view of multi-annual changes in phytoplankton dynamics and the various interacting processes, the Scheldt
57 estuary is an interesting example. A phytoplankton spring (Apr-May) bloom appeared and disappeared in the brackish
58 region (km 60-90 from the mouth, salinity \sim 1-10 ppt) between 2004-2018 (Maris and Meire, 2017). From 2004
59 until 2007, almost no spring bloom was observed in the brackish region. A spring bloom was consistently observed
60 between 2008-2014 but disappeared after 2015. Covering the same period, Cox et al. (2019) reported a multi-annual
61 estuary-scale change in SPM dynamics in the Scheldt estuary in summer and winter. From 2009 onwards, a change
62 in the estuarine turbidity maximum dynamics (e.g., the appearance of a new turbidity maximum in winter) and an
63 overall increase in SPM concentration were observed. Simultaneously, the water quality in the Scheldt estuary improved
64 drastically (e.g., reduction of ammonium), mainly because of a significant increase in wastewater treatment capacity
65 in Brussels around 2006 (Brion et al., 2015). This resulted in increasing oxygen concentrations and changes in the
66 zooplankton community and abundance. In 1996, calanoid copepods, in casu *Eurytemora affinis*, dominated in the
67 downstream brackish region and were quasi absent (time-average < 1 ind. L^{-1}) in the freshwater region (> 90 km from
68 the mouth). From 2007, they gradually developed more upstream to also become dominant there in 2009 (Appeltans,
69 2003; Mialet et al., 2010, 2011; Chambord et al., 2016). The reported changes in SPM in summer and winter and
70 zooplankton dynamics have been hypothesized to link to the multi-annual disappearance of phytoplankton blooms in
71 spring (Maris and Meire, 2017). However, this has not been systematically investigated, which is necessary given the
72 complex interplay between factors affecting phytoplankton growth. In this contribution, we aim to quantify the relative
73 impact of various factors affecting phytoplankton dynamics on the appearance and disappearance of the phytoplankton
74 bloom in the brackish zone in the Scheldt estuary. To this end, we apply a modeling approach in which observations
75 are the core.

76 As discussed by Franks (2009), the choice of an appropriate modeling approach to acquire insight into the
77 phytoplankton(-zooplankton) dynamics depends on the research questions and data availability. Arndt et al. (2011),
78 Naithani et al. (2016), and Gypens et al. (2013) explicitly resolved the phytoplankton-zooplankton(-nutrient) dynamics
79 over one year in the Scheldt estuary using a complex model (from a biochemical perspective) that includes multiple
80 phytoplankton and zooplankton groups. This resulted in valuable insight into the transient behavior of phytoplankton
81 and zooplankton groups covering the full estuary in 1995, 2003, and 2006, respectively. However, using such models to
82 study multi-annual changes is challenging. The main reason is that (long-term) experimental data is often unavailable,
83 which has three important consequences. Firstly, some of the modeled planktonic groups cannot be observationally
84 validated. Secondly, such models require many (\sim dozens) calibration parameters that are often poorly constrained
85 (e.g., maximum grazing rate, mortality rate per species). These parameters are generally calibrated by fitting them to
86 data and assumed to be fixed in time. Although assuming fixed parameters may be acceptable when focusing on one
87 year, this assumption may be invalid when interested in multi-annual trend changes, suggesting that (some of these)
88 parameters must have changed over time. Thirdly, different model input parameter choices may lead to similar model
89 results, which is known as equifinality. Equifinality has been studied using sediment-transport (van Maren and Cronin,
90 2016) and planktonic ecosystem models (Friedrichs et al., 2006, 2007) applied to estuarine and marine systems. This
91 phenomenon especially occurs when using more complex models (e.g., including more processes) because the number
92 of model parameters increases by as much as the square of the number of state variables (Denman and Pea, 2002).

93 To avoid such problems as much as possible, we choose our model such that it is mainly data-driven and most of its
94 parameters directly follow from observations. We aim to minimize the number of variables and calibration parameters
95 that we cannot directly observe. This requires the combining of several biological factors into lumped parameters
96 related to SPM characteristics, phytoplankton properties, and zooplankton grazing. By calibrating these parameters
97 for different years, we can determine which of the combined sets of processes may explain the observed changes.

98 This contribution is structured as follows. We first introduce the model approach, the Scheldt estuary, and the
99 methodology to obtain the observations in Section 2. In Section 3, we show the multi-annual observations of Chl-a
100 and factors impacting phytoplankton growth in the Scheldt estuary in spring. Next, we present the results of our model
101 experiments: we calibrate the model, apply a sensitivity analysis of factors that may explain the disappearance of
102 phytoplankton accumulation in the brackish region, and run different model scenarios. We study whether this multi-
103 annual trend in phytoplankton accumulation may be constrained by an individual multi-annual change in grazing by

104 zooplankton or other processes contributing to the phytoplankton mortality rate. In Section 4, we discuss the data and
 105 model results and modeling approach. Finally, we conclude in Section 5.

106 2. Material and methods

107 In this section, we introduce the core characteristic of our data-driven modeling approach necessary to understand
 108 our modeling sensitivity study and model scenarios. Next, we explain how the necessary data used in the model was
 109 obtained. Finally, we present four model scenarios to study the individual effect of multi-annual changes in SPM and
 110 phytoplankton and zooplankton characteristics on the multi-annual evolution of phytoplankton.

111 2.1. Model set-up

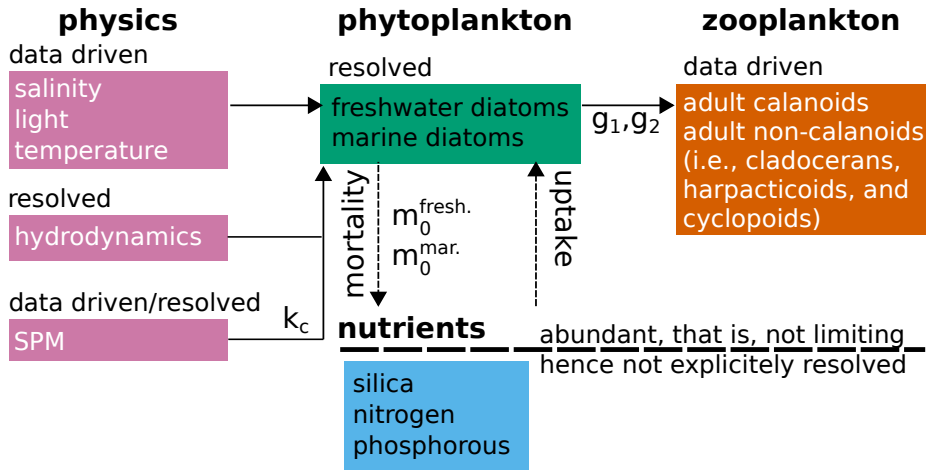


Figure 1: A schematic overview of the physical-biochemical factors that affect phytoplankton dynamics and phytoplankton and zooplankton classes that are included in our model approach.

112 We present a schematic overview of the physical-biochemical factors that affect phytoplankton dynamics and are
 113 included in our model approach in Fig. 1. The (lumped) calibration parameters are related to phytoplankton- (i.e., $m_0^{\text{fresh.}}$,
 114 $m_0^{\text{mar.}}$) and zooplankton characteristics (i.e., g_1 , g_2). These parameters are subject to extensive sensitivity study when
 115 we consider four model scenarios (see Section 2.3). Here, we also focus on a parameter related to SPM characteristics
 116 (i.e., k_c). The model scenarios allow us to quantify the individual impact of potential multi-annual changes in SPM,
 117 phytoplankton, and zooplankton characteristics on the multi-annual evolution of phytoplankton accumulation in the
 118 brackish region, which is the aim of this contribution. We choose to implement our modeling set-up in the process-
 119 based, width-averaged model iFlow (Dijkstra et al., 2017). For additional technical details, we refer the reader to
 120 Dijkstra et al. (2017, 2019a), Horemans et al. (2020a), and the Supporting Information. In the following sections, we
 121 briefly describe each box presented in Fig. 1 and define the corresponding parameters of interest.

122 2.1.1. Phytoplankton

123 Cell count observations show that the dominant phytoplankton species in the Scheldt estuary in spring are diatoms
 124 and not chlorophytes or other algae groups (euglenophytes, cryptophytes, cyanobacteria, and dinophytes) (Maris and
 125 Meire, 2007; Muylaert et al., 2009; Maris and Meire, 2009, 2013, 2017). We distinguish between freshwater and marine
 126 diatoms because salt stress is considered to have an important effect (Gypens et al., 2013). Besides the effect of salinity
 127 stress, each diatom class has a unique maximum growth and mortality rate. Processes causing phytoplankton mortality
 128 are subdivided into two classes: zooplankton grazing and all other processes. The latter is parameterized by lumped
 129 parameters $m_0^{\text{fresh.}}$ and $m_0^{\text{mar.}}$ for the freshwater and marine diatoms, respectively.

130 We adapted iFlow's phytoplankton module (Dijkstra et al., 2019a). The width-averaged differential equation for
 131 the phytoplankton concentration P^i of phytoplankton group i and corresponding boundary conditions read as (Dijkstra
 132 et al., 2019a)

$$\underbrace{\partial_t P^i + u \partial_x P^i + (w - w_p) \partial_z P^i - \frac{1}{B} \partial_x (B K_h \partial_x P^i) - \partial_z (K_v \partial_z P^i)}_{\text{advection-diffusion}} = \underbrace{(\mu - m) P^i}_{\text{balance between local growth and mortality}}, \quad (1)$$

$$\begin{cases} w_p P^i + K_v \partial_z P^i = 0, & \text{at the bed and water surface (no flux),} \\ \left\langle \frac{1}{H+\zeta} \int_{-H}^{\zeta} P^i dz \right\rangle = P_{\text{sea}}, & \text{at the seaside boundary (constant concentration),} \quad \text{and} \\ B \left\langle \int_{-H}^{\zeta} (u P^i - K_h \partial_x P^i) dz \right\rangle = QP, & \text{at the upstream boundary (constant influx).} \end{cases} \quad (2)$$

133 Here, t represents time, x and z are the coordinates in the longitudinal and vertical direction, respectively, u and w
 134 are the water velocities in the longitudinal and vertical direction, w_p is the constant settling velocity of phytoplankton
 135 cells, B is the width of the estuary, K_h and K_v are the horizontal and vertical eddy diffusivities, the angle brackets
 136 denote averaging over a long time scale (i.e., larger than a tide or day; 15 days), $-H$ and ζ are the z -coordinates of the
 137 bed and water surface, P_{sea} is the constant phytoplankton concentration at the seaside boundary, QP is the constant
 138 influx of phytoplankton at the upstream boundary, and μ and m are the growth and mortality rate of phytoplankton.
 139 We divide the model into two phytoplankton classes: freshwater diatoms P^{fresh} and marine diatoms P^{mar} . Following
 140 Naithani et al. (2016), most parameters of the two phytoplankton groups are equal, except the mortality rate m and
 141 maximum growth rate μ_{max} [defined in Eq.(6)], which is ~ 1.6 times larger for marine diatoms. The mortality rate
 142 depends on salinity S and the abundance of phytoplankton grazers Z :

$$m = m_0^i f_S(S) + f_Z(Z), \quad (3)$$

143 in which m_0^i is a (calibrated) constant mortality rate parameter of phytoplankton group i (i.e., the freshwater or marine
 144 diatoms) and f_S and f_Z are functions that determine the salinity and zooplankton dependence of the mortality rate m ,
 145 respectively. Following Naithani et al. (2016), we assume the following (normalized) salinity stress:

$$f_S(S) = \begin{cases} \frac{1.07^S}{1.07^{\text{ssea}}}, & \text{freshwater diatoms,} \\ \frac{1+5 \times 0.85^S}{1+5 \times 0.85^{\text{upstream}}}, & \text{marine diatoms,} \end{cases} \quad (4)$$

146 in which ssea and S^{upstream} are the salinity at the downstream and upstream boundary (in ppt), respectively. In the
 147 literature, multiple zooplankton dependencies of the phytoplankton mortality rate have been studied (Steele and
 148 Henderson, 1992). We consider the following longitudinal variation in m due to zooplankton abundance:

$$f_Z(Z^j) = \sum_j g_j Z^j(x) \quad (5)$$

149 in which g_j is a grazing parameter corresponding to zooplankton class j that follow from calibration (units $\text{s}^{-1} \text{L}$
 150 ind.^{-1}).

151 Given that the Scheldt estuary is a turbid system, we use the Platt formulation for light limitation of the time-
 152 averaged growth rate μ (Platt et al., 1980). This formulation is suitable for turbid systems as it does not consider an
 153 inverse relationship between μ and the photosynthetically active radiation E at large E (cf. cell burning). Without
 154 nutrient limitation, μ then reads

$$\mu = \mu_{\text{max}}(T) \left\langle \underbrace{\left[1 - \exp\left(-\frac{\alpha}{P_{\text{max}}} E\right) \right]}_{\text{Platt light limitation}} \right\rangle, \quad (6)$$

155 in which T is the water temperature, P_{\max} is the maximum photosynthetic rate, α is the growth efficiency, the angle
 156 brackets again denote averaging over a long time scale (i.e., larger than a tide or day; 15 days) to average out interference
 157 between the daily and tidal cycle, and μ_{\max} is the maximum growth rate. Following Eppley (1972), we postulate the
 158 following temperature dependence of the maximum growth rate $\mu_{\max}(T)$:

$$\mu_{\max}(T) = \mu_{00} \mu_{01}^{\left(\frac{T}{10^\circ\text{C}}\right)}, \quad (7)$$

159 in which μ_{00} and μ_{01} are calibration parameters and T is expressed in $^\circ\text{C}$. The photosynthetically active radiation E
 160 reads as

$$E(x, z, t; P^i, c) = \hat{E}_{00}(t) \underbrace{\exp\left(-k_c \int_z^0 c(x, z, t) dz\right)}_{\text{SPM-induced light extinction}} f_I(x, z, t; P^i), \quad (8)$$

161 in which \hat{E}_{00} represents the photosynthetically active radiation (PAR) at the water surface, c is the SPM concentration,
 162 k_c is the SPM-induced exponential light extinction coefficient, and f_I corresponds to exponential light extinction due
 163 to background effects (e.g., absorption by water molecules) and self-shading by phytoplankton cells. For the definition
 164 of \hat{E}_{00} and f_I , we refer the reader to the Supporting Information.

165 The model solves the approximated phytoplankton dynamics in equilibrium conditions (Dijkstra et al., 2019a),
 166 that is, the state reached after a sufficiently long time of constant forcing, thus representing long-term trends rather
 167 than transient behavior. By doing so, we do not have to postulate initial conditions, which further simplifies our
 168 sensitivity analysis. We argue that this assumption of equilibrium conditions is acceptable because the accumulation
 169 of phytoplankton in the brackish region covers approximately two months, which is large compared to the time scale
 170 of a bloom (~ 2 -3 weeks). As shown by Regnier et al. (1997), the accuracy of their coupled reaction-transport in
 171 equilibrium conditions applied to the Scheldt estuary depends on the biological rates; higher rates (which are typical for
 172 the spring/summer months) result in higher model performance. We solve the marine and freshwater diatom dynamics
 173 separately and thereby neglect their coupling through shading by marine diatoms on freshwater diatoms and vice versa.
 174 This assumption is acceptable as we show later that freshwater and marine diatoms are spatially separated. In the region
 175 where we have similar concentrations of freshwater and marine (cf. coupling), self-shading is negligible. Last, for the
 176 implementation of time-averaged μ , we use the approximated Platt light limitation function presented in Horemans
 177 et al. (2020b). By solving approximate solutions for the phytoplankton dynamics, our model approach comes with
 178 very low computation times (\sim s) when compared to more realistic models (\sim hours-days), allowing for an extensive
 179 sensitivity analysis.

180 The variables required to solve our phytoplankton model are salinity (S), PAR at the water surface (\hat{E}_{00}), water
 181 temperature (T), water flow velocity (u and w) and surface elevation (ζ), SPM concentration (c), and zooplankton
 182 abundance (Z). The next subsections are about these variables.

183 2.1.2. Salinity, light, and temperature

184 Salinity, light at the water surface, and temperature all impact phytoplankton growth and are considered data-driven
 185 variables in our model. They thus directly follow from observations. Following Warner et al. (2005), the longitudinal
 186 salinity profile is implemented as a tide- and depth-independent profile (see the Supporting Information attached to
 187 this paper). This assumption is consistent with the Scheldt estuary being well-mixed (Baeyens et al., 1997).

188 2.1.3. Hydrodynamics

189 The vertical and longitudinal water flow velocity and water surface elevation are resolved by solving the width-
 190 averaged shallow water equations in equilibrium conditions. For this, we use an equidistant grid of 100 cells in
 191 the longitudinal and 50 in the vertical direction. The model focuses on the estuary-scale hydrodynamics only by
 192 approximating the estuary's bathymetry and width by smooth profiles. The model resolves the tidal and subtidal
 193 dynamics of water motion and provides approximate solutions of the complex and nonlinear set of equations for
 194 hydrodynamics using a scaling and perturbation approach. The hydrodynamics are forced at the upstream boundary
 195 and two main tributaries by a fixed water inflow and at the mouth by a tidal signal.

2.1.4. SPM

Knowing the SPM concentration is important because it determines the PAR E in the water column and the corresponding SPM-induced exponential light extinction coefficient k_c . The SPM concentration follows from a combined model and data-driven approach.

Similarly to the hydrodynamics, the model solves for cohesive SPM trapping in tide-dominated estuaries by resolving the width-averaged SPM mass balance equations in equilibrium condition using the same model grid. The SPM dynamics are forced by a constant inflow of SPM that equals the product of the water discharge and subtidal SPM concentration at the upstream boundary, and by a fixed SPM concentration at the mouth. We assume that erosion of sediment scales to the magnitude of the bed shear stress. The flocculation dynamics of cohesive SPM are resolved using a single-class dynamic flocculation model (Winterwerp, 2002; Horemans et al., 2020a). Following Horemans et al. (2020a), we calibrate the erosion and flocculation characteristics by calibrating the subtidal SPM model output to the corresponding multi-annual subtidal SPM observations. Because SPM changes due to dredging and dumping activities, which are not included in the model, may be locally important (Brouwer et al., 2018; Dijkstra et al., 2019b; Horemans et al., 2020a), we partly follow a data-driven approach. We add a background SPM concentration following from the SPM observations at the dumping locations to our modeled SPM concentrations (see Supporting Information for the technical details).

2.1.5. Zooplankton

Observed zooplankton abundances are directly used in the model and not resolved dynamically, hence eliminating the uncertainty of a dynamic zooplankton model. Observations allow us to distinguish between two dominant zooplankton groups calanoids $Z^{\text{calanoids}}$ and non-calanoids $Z^{\text{non-calanoids}}$ (units ind. L^{-1} , where ‘ind.’ denotes ‘individuals’), where calanoids are dominant in the brackish region in spring (Appeltans, 2003; Mialet et al., 2011). More specifically, we linearly interpolate the zooplankton abundance observations and extrapolate the zooplankton abundance in the downstream region where we do not have observations using the system-averaged abundance. Assuming these two zooplankton groups, Eq. (5) then reads as

$$f_Z(Z^{\text{calanoids}}, Z^{\text{non-calanoids}}) = g_1 Z^{\text{calanoids}}(x) + g_2 Z^{\text{non-calanoids}}(x), \quad (9)$$

in which g_1 , and g_2 are grazing parameters that follow from calibration (units $\text{s}^{-1} \text{L ind.}^{-1}$).

2.1.6. Nutrients

We do not focus on nutrient (and detritus) dynamics because the Scheldt estuary is a nutrient-rich estuary (Cox et al., 2009; Maris and Meire, 2017). The time-averaged dissolved nitrogen, phosphorous, and silicon concentrations in spring range from 0.1 mmol L^{-1} , $0.001 \text{ mmol L}^{-1}$, and $0.005 \text{ mmol L}^{-1}$ at the seaside boundary to 0.4 mmol L^{-1} , $0.007 \text{ mmol L}^{-1}$, and 0.13 mmol L^{-1} at the upstream boundary, respectively. These concentrations are at least one order of magnitude larger than the half-saturation constants at which we expect nutrient depletion (Billen and Garnier, 1997; Lancelot et al., 2005; Arndt et al., 2011; Naithani et al., 2016). At the downstream boundary, the phosphorous and silicon concentrations may approach the order of the half-saturation constant temporarily. However, just 20 km from the mouth (which is still 40 km downstream from the brackish region of interest), these concentrations are always significantly larger than the concentrations at which we expect nutrient limitation. We also do not explicitly consider the effect of nutrient ratios on the phytoplankton community (Sterner and Elser, 2017).

2.1.7. Calibration and parameter values

In this section, we summarize the calibration procedures and parameter values used in this contribution. For the technical details and full parameter list, we refer the reader to the Supporting Information. We combine our modeled and data-driven SPM distributions with observations of vertical light extinction to estimate the SPM-induced light extinction coefficient k_c . We quantify the grazing parameters g_1 and g_2 corresponding to the calanoids and non-calanoids, respectively, and mortality rate parameters $m_0^{\text{fresh.}}$, $m_0^{\text{mar.}}$ corresponding to freshwater and marine diatoms, respectively, by calibrating modeled Chl-a concentrations to the Chl-a observations. Here, we use the calibration method described in Horemans et al. (2020a) in which the phytoplankton model results and observations (cf. Chl-a) are quantitatively compared. Using the observed P_{max} and temperature, we derive the calibration parameters μ_{00} and μ_{01} defined in Eq. (7). The influx of phytoplankton at the upstream boundary QP follows from the Chl-a observations at the upstream boundary. The model parameters that are the focus of this paper are summarized in Table 1.

Table 1

Selection of parameter values used in our model experiments based on observations (obs), model calibration (calibrated), and the literature. For a complete list, we refer the reader to the Supporting Information.

Variable	Definition	Value			Unit
		2004-2007	2008-2014	2015-2018	
k_c	SPM-induced exponential light extinction coefficient (obs)	81.4	77.9	72.0	$\text{m}^2 \text{kg}^{-1}$
$m_0^{\text{fresh.}}$	Mortality rate parameter for freshwater diatoms (calibrated)	1.89×10^{-6}	3.30×10^{-6}	8.30×10^{-6}	s^{-1}
$m_0^{\text{mar.}}$	Mortality rate parameter for marine diatoms (calibrated)	3.21×10^{-6}	1.06×10^{-6}	3.35×10^{-6}	s^{-1}
g_1	Calanoids grazing parameter (calibrated)	0.8×10^{-7}	0.13×10^{-7}	0.8×10^{-7}	$\text{s}^{-1} \text{L ind.}^{-1}$
g_2	Non-calanoids grazing parameter (calibrated)	0.47×10^{-7}	0.32×10^{-7}	0.47×10^{-7}	$\text{s}^{-1} \text{L ind.}^{-1}$
$\mu_{00}^{\text{fresh.}}$	Maximum growth rate at 0 ° C of freshwater diatoms (obs)	0.96×10^{-5}	1.04×10^{-5}	0.86×10^{-5}	s^{-1}
$\mu_{00}^{\text{mar.}}$	Maximum growth rate at 0 ° C of marine diatoms (obs)	1.59×10^{-5}	1.72×10^{-5}	1.43×10^{-5}	s^{-1}
P_{sea}	Phytoplankton boundary concentration at the mouth (obs)	15.9	17.1	15.8	$\mu\text{g L}^{-1}$
QP	Influx of phytoplankton at the upstream boundary (obs)	1.5	1.8	2.5	g s^{-1}

2.2. In situ observations

The Scheldt estuary is a funnel-shaped estuary that flows through Belgium into the North Sea near Vlissingen (Netherlands) over a distance of approximately 160 km (Fig. 2). Given its relatively small freshwater discharge compared to the tidal volumes, the Scheldt estuary is tide-dominated (Baeyens et al., 1997; Meire et al., 2005). The total time-averaged freshwater discharge Q in spring (Apr.-May) equaled 85, 81, and 72 $\text{m}^3 \text{s}^{-1}$ in 2004-2007, 2008-2014, and 2015-2018, respectively (Waterinfo.be, cited 2019, gauge station *zes29f-1066* ~ 1 km downstream from the Rupel tributary). The main tributaries of the Scheldt estuary are the Rupel and the Dender. They are responsible for 64.2, 59.3, 63.3 % and 9.4, 9.2, 9.6 % of the total river discharge in 2004-2007, 2008-2014, and 2015-2018, respectively (Waterinfo.be, cited 2019, deducted from gauge stations at the upstream boundary *zes57a-1066*, at the Dender tributary *den02a-1066*, and downstream from the Rupel tributary *zes29f-1066* assuming no water leaves or enters the Scheldt estuary in between these stations).

Both the Belgian and Dutch part of the Scheldt estuary have been monitored intensively over the last two decades. In the Belgian region, various variables have been measured within the multi-annual OMES (Dutch: “Onderzoek Milieu Effecten Sigmaphan”) monitoring program (Maris and Meire, 2017), independently of the tidal phase and spring-neap tide biweekly or monthly at 16 fixed stations (Fig. 2). These variables include Chl-a, zooplankton abundance, SPM, light extinction, salinity, and phytoplankton characteristics, such as the maximum photosynthetic rate P_{max} and growth efficiency α . In the Dutch region, we only use observations of Chl-a and SPM conducted by Rijkswaterstaat at three stations in the main channel (Fig. 2). In the following, we briefly introduce the methodology used to obtain the observations presented in this contribution. For a detailed methodological description, we refer the reader to the OMES reports (Maris and Meire, 2017) and the website of Rijkswaterstaat (Rijkswaterstaat, 2020).

2.2.1. Chl-a and zooplankton abundance

Within the OMES monitoring program, sub-surface bucket samples were taken to estimate the Chl-a concentration and the mesozooplankton abundance between 2004-2018. The Chl-a concentration was estimated following the spectrophotometric method described in Rice et al. (2017) that corrects for turbidity, Chlorophyll-b, Chlorophyll-c, and Pheophytin pigments, using 50 ml water samples, a 1-cm pathway cuvette, and a Shimadzu UV-1700 spectrophotometer (wavelength range 190 to 1100 nm). The observations conducted by Rijkswaterstaat in the Dutch part of the Scheldt estuary were estimated using High-performance liquid chromatography (HPLC) after filtration (0.2 μm filter) and extraction (90 % acetone).

To estimate the mesozooplankton abundance, 50-250 L sub-surface water samples were collected and filtered over a 50 μm mesh. Next, the mesozooplankton was fixed using formaldehyde and stained with erythrosine in the laboratory. Finally, the organisms were counted in a counting wheel under a binocular microscope using a subsample. A minimum of 500 individuals per subsample was counted (Le Coz et al., 2017). Following Mialet et al. (2011), we divide the mesozooplankton abundance observations at genera level for cladocerans and at phylum level for copepods (cyclopoids, calanoids and harpacticoids). In the brackish region in spring, which is the main focus of this paper, the mesozooplankton community dominantly consists of calanoids (Appeltans, 2003; Mialet et al., 2011). Therefore, also

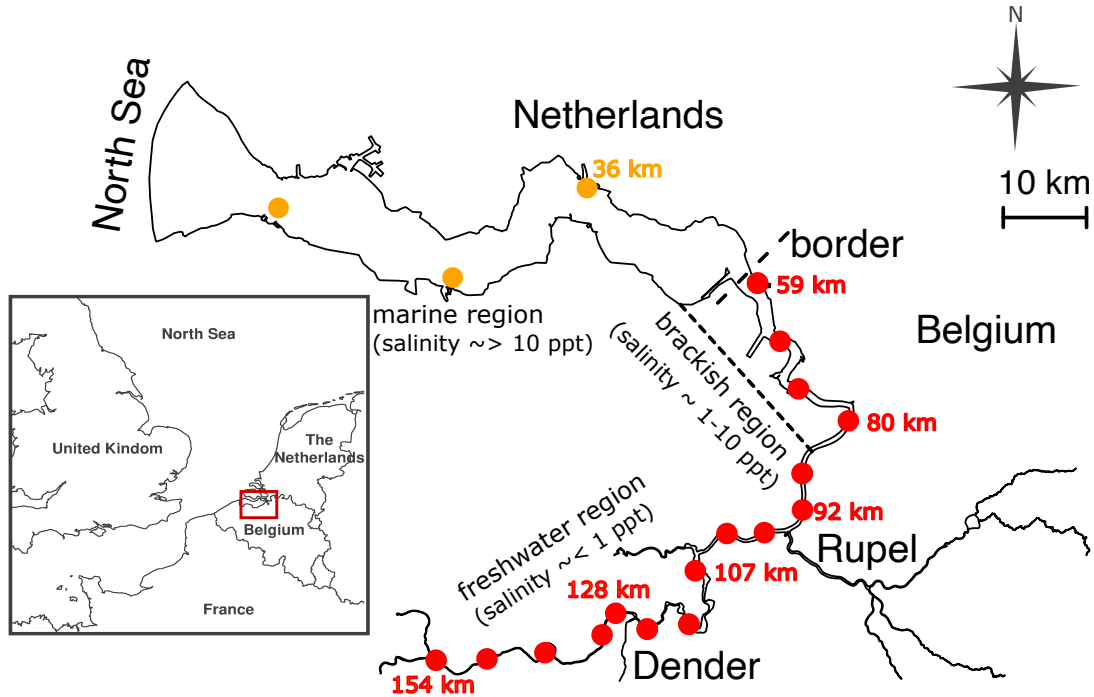


Figure 2: The Scheldt estuary and its two main tributaries (Rupel and Dender). The red dots represent the locations where was sampled monthly and biweekly in the frame of the OMES environmental monitoring program. The orange dots depict the locations of the observations conducted by Rijkswaterstaat.

278 given our modeling philosophy that aims to minimize the number of variables and calibration parameters that we cannot
 279 directly observe, we divide the community into two groups: adult calanoids and adult non-calanoids (i.e., cladocerans,
 280 harpacticoids, and cyclopoids).

281 2.2.2. Turbidity and SPM concentration

282 Within the OMES campaign, turbidity depth profiles were measured in 2015-2018 using an Optical Backscatter
 283 point Sensor (OBS) of RBR type XR420 CTD+ at the 16 OMES stations. Simultaneously, two SPM samples were
 284 collected at approximately the water surface and half the water depth. These SPM samples were used to translate
 285 turbidity to SPM concentration (a linear fit was applied each campaign; Horemans et al., 2020a). The number of spring
 286 campaigns between 2015-2018 equals 16.

287 To determine the SPM concentration, 1 L water samples were collected and filtered in the laboratory using a GF/C
 288 50 mm filter. To remove salinity, the filters were rinsed with 3×50 ml demineralized water before gravimetrically
 289 determining the SPM concentrations (norm NBN-EN872). Also within the monitoring program of Rijkswaterstaat,
 290 SPM concentrations were gravimetrically determined after filtration on a glass microfiber filter.

291 2.2.3. Light extinction coefficients and salinity

292 The light climate was measured by estimating the light extinction coefficient k_d . Two light sensors (LiCOR)
 293 measured the light intensity near the water surface E_1 and the light-intensity E_2 at a fixed distance $\Delta z = 40$ cm
 294 from the sub-surface sensor. Next, the light extinction coefficient was estimated as $k_d = \log(E_1/E_2)/\Delta z$, assuming
 295 exponential decrease of light as a function of depth. To correct for small-scale temporal variability (cf. seconds) in
 296 the light climate, the time-averaged value of k_d was estimated over a time interval of 3-5 minutes, using a sampling
 297 frequency of 1 s^{-1} (Maris and Meire, 2017). An estimate at the water surface suffices because, given the high turbidity
 298 in the Scheldt estuary, the euphotic depth is relatively small (\sim dm) compared to the mixing depth (\sim m). We thus
 299 expect phytoplankton growth only near the water surface, where we do not expect strong vertical stratification of SPM.

Specific conductivity was determined in situ using a WTW LF 318 instrument directly after taking the bucket samples. Specific conductivity was transformed to salinity using the Practical Salinity Scale 1978 (Perkin and Lewis, 1980).

2.2.4. Photosynthetic parameters

To estimate the maximum photosynthetic rate P_{\max} and growth efficiency α , the incubation method described in Kromkamp and Peene (1995) was applied using the incubator presented in Vegter and De Visscher (1984) and assuming a photosynthesis–irradiance (P-I) curve introduced in Eilers and Peeters (1988). Briefly explained, the Chl-a concentration was determined and water samples from various stations in Belgian part of estuary were placed at fixed distances from a constant light source. Each distance thus corresponds to a given solar irradiance I . Next, the water samples were incubated for approximately 2 hours, while gently being rotated to avoid settling. The photosynthesis was determined using a C-14 isotope method; radioactive $\text{NaH}^{14}\text{CO}_3$ was added to each sample and the amount of dissolved CO_2 was determined at each I , resulting in an estimate of the amount of carbon that is uptaken per unit of time per unit of Chl-a. Finally, a P-I curve was constructed to estimate P_{\max} and α .

2.3. Model scenarios

To study the individual impact of potential multi-annual changes in SPM and phytoplankton and zooplankton characteristics on the multi-annual evolution of Chl-a accumulation, we consider four model scenarios:

1. We calibrate the parameters $m_0^{\text{fresh.}}$, $m_0^{\text{mar.}}$, g_1 , and g_2 for the three distinct periods and determine the minimal multi-annual change in these calibration parameters required to capture the accumulation of Chl-a in the brackish region in spring.
2. We test what multi-annual change in SPM characteristics (i.e., k_c) is required to capture the accumulation of Chl-a in 2008-2014 in the brackish region assuming no multi-annual change in $m_0^{\text{fresh.}}$, $m_0^{\text{mar.}}$, g_1 , and g_2 after 2007.
3. We assume a dominant impact of grazing by zooplankton on the mortality rate (i.e., $m_0^{\text{fresh.}} = 0$ and $m_0^{\text{mar.}} = 0 \text{ s}^{-1}$) and test what multi-annual change in grazing parameters (i.e., g_1 and g_2) is required to capture the multi-annual evolution of Chl-a accumulation.
4. We neglect the impact of grazing by zooplankton on the mortality rate (i.e., $g_1 = 0$ and $g_2 = 0 \text{ s}^{-1} \text{ L ind.}^{-1}$) and test what multi-annual change in the mortality rate parameters (i.e., $m_0^{\text{fresh.}}$ and $m_0^{\text{mar.}}$) is required to capture the multi-annual evolution of Chl-a accumulation.

3. Results

3.1. Evolution of Chl-a and corresponding environmental conditions of the in situ observations

3.1.1. Evolution of Chl-a and zooplankton

The sub-surface Chl-a concentration in 2004-2018 shows a clear seasonality and corresponding phytoplankton blooms (Fig. 3a); at the upstream boundary (\sim km 160, salinity \approx 0 ppt), the Chl-a concentration can reach values above $400 \mu\text{g L}^{-1}$ in summer and, although local maxima are observed, decays in the downstream direction. We divide the time series into three distinct periods and focus on the time-averaged Chl-a concentration in spring (Apr.-May) (Fig. 3b). In 2004-2007, we detect time-averaged Chl-a concentrations above $50 \mu\text{g L}^{-1}$ in the upstream region, $>$ km 80. In 2008-2014 and 2015-2018, this region is limited to $>$ 100 km and $>$ 110 km, respectively. In 2008-2014, we also observe concentrations $>$ $50 \mu\text{g L}^{-1}$ more downstream in the brackish region between km 60-90. The Chl-a concentrations are significantly larger in 2008-2014 in the brackish region compared to the concentrations in 2004-2007 (Welch t-test, p-value $<$ 10^{-3}) and 2015-2018 (Welch t-test, p-value $<$ 10^{-12}).

The time-averaged calanoids and non-calanoids abundance in spring for the three distinct periods considered is presented in Fig. 4. The shaded area depicts the standard error of the zooplankton abundance. The calanoids abundance (Fig. 4a) also shows distinct trends in the three periods considered. In 2004-2007, we observe a relatively low mean calanoids abundance between km 110-150, ranging up to approximately 5 ind. L^{-1} . Downstream from km 110, we observe an increase in calanoids, resulting in a local maximum of the mean values of calanoids of approximately 10 ind. L^{-1} , centered near km 90. In 2008-2014, the local maximum of the mean values in calanoids abundance shifts in the upstream direction and increases. The overall calanoid abundance increases, with a maximum of the mean values of approximately 17.5 ind. L^{-1} at km 110. In 2015-2018, the local maximum of the mean values in calanoids abundance shifts further landwards to approximately km 140, with again a maximum of approximately 17.5 ind. L^{-1} .

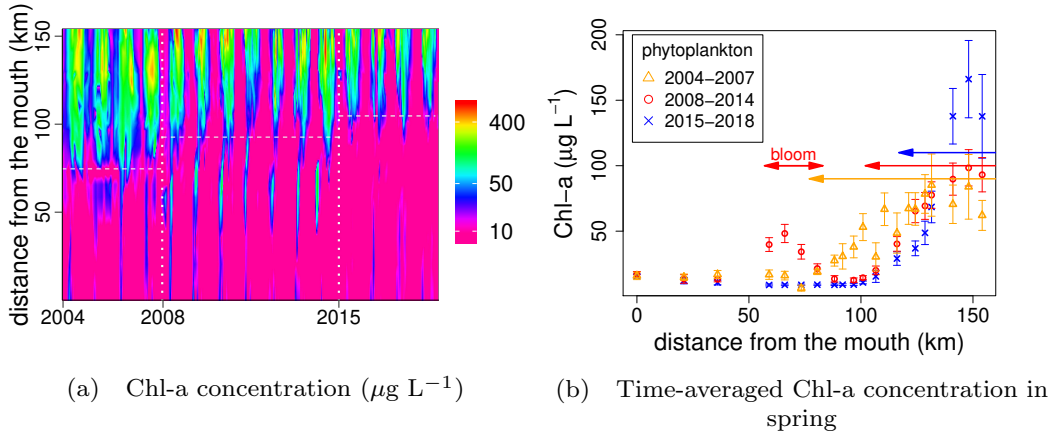


Figure 3: (a) Observed Chl-a concentration ($\mu\text{g L}^{-1}$) in 2004–2018 and (b) time-averaged Chl-a concentration in spring. We observe a phytoplankton bloom in the brackish region (km 60–90) in spring in 2008–2014, which is absent in the other years considered. The Chl-a concentration also decreases faster in the downstream direction in more recent years (illustrated by the horizontal arrows). The geographical locations of the measuring stations are depicted in Fig. 2.

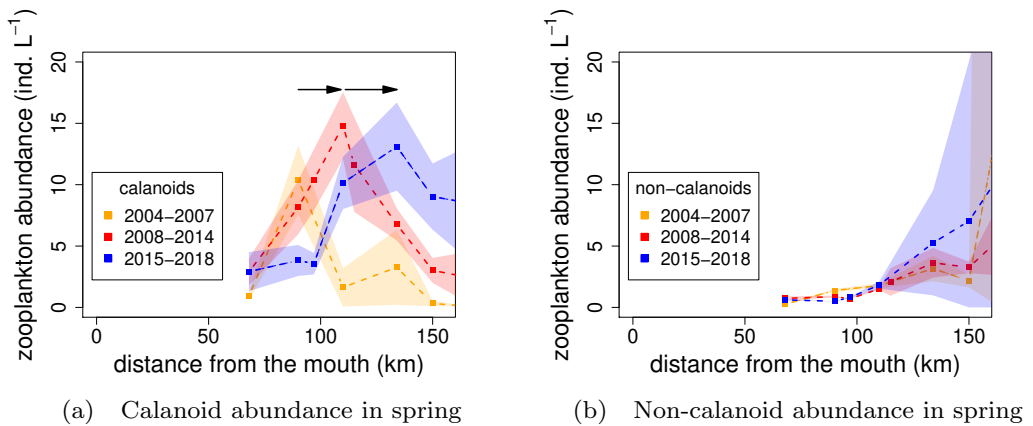


Figure 4: Multi-annual time averages of (a) calanoids and (b) non-calanoids abundance in spring (Apr.–May). The shaded area depicts the standard error. We observe a dominant abundance of calanoids in the brackish region and a land-inward shift of calanoids in time. The non-calanoids are mainly situated at the upstream boundary. The geographical locations of the measuring stations are depicted in Fig. 2.

349 We thus observe a land-inward shift and estuary-scale increase of the local calanoids concentration over time. The
 350 calanoids concentrations are significantly larger between km 110–150 in 2015–2018 compared to 2004–2007 (Welch
 351 t-test, p-value $< 10^{-4}$). At the upstream boundary, non-calanoids are dominantly present (Fig. 4b). On average, we
 352 observe an increase of the non-calanoids abundance in the landward direction on the estuary scale in all three periods.
 353 As illustrated by the large standard error, the differences of the non-calanoids abundance are not statistically significant
 354 between the three distinct periods (Welch t-test, p-value = 0.10 and 0.22 when comparing the abundances between km
 355 110–150 in 2015–2018 to 2004–2007 and 2008–2014, respectively).

3.1.2. Evolution of SPM and light extinction

In all three periods in spring, the sub-surface time-averaged SPM concentrations range up to approximately 150 mg L^{-1} (Fig. 5a). However, we observe significantly lower concentrations between approximately km 50-100 in 2004-2007 (Welch t-test, p-value $< 10^{-5}$ and $< 10^{-6}$ when compared to 2008-2014 and 2015-2018, respectively). The lower SPM concentrations are especially visible between km 70-80, where we have concentrations below 50 mg L^{-1} in 2004-2007 and up to 150 mg L^{-1} after 2007. Moreover, in 2015-2018, we observe the largest SPM concentrations between km 80-120 (Welch t-test, p-value $< 10^{-3}$ and $< 10^{-4}$ when compared to 2008-2014 and 2004-2007, respectively).

The time-averaged light extinction coefficient in spring shows a similar evolution to the SPM concentration (Fig. 5b), with significantly lower values of approximately 4 m^{-1} between km 50-100 in 2004-2007 compared to the values of approximately 7 m^{-1} after 2007 (Welch t-test, p-value $< 10^{-8}$ and $< 10^{-10}$ when compared to 2008-2014 and 2015-2018, respectively). We have the largest time-averaged values between km 80-120 in 2015-2018, which is consistent with the SPM observations (Welch t-test, p-value = 3.4×10^{-2} and $< 10^{-5}$ when compared to 2008-2014 and 2004-2007, respectively).

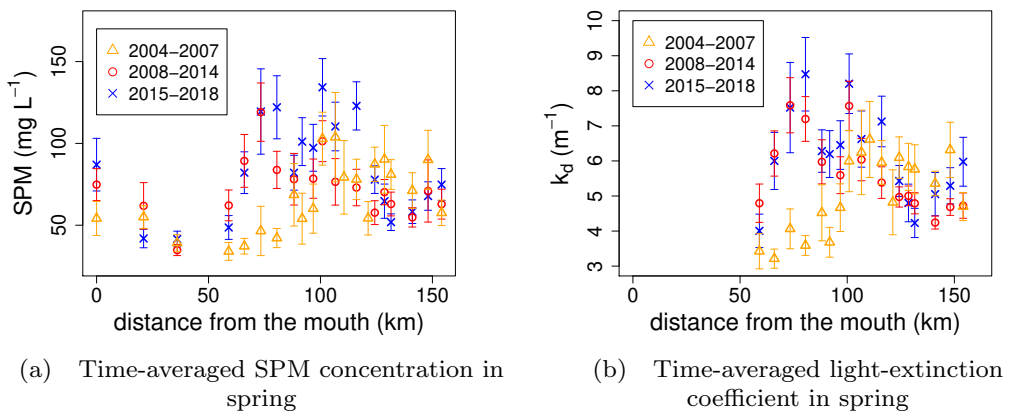


Figure 5: Multi-annual time-averaged observations in spring (Apr.-May) in 2004-2018 of (a) the water surface SPM concentration and (b) the light extinction coefficient k_d . The error bars depict the standard error of the observations. The geographical locations of the measuring stations are depicted in Fig. 2.

3.1.3. Evolution of discharge, salinity intrusion, and photosynthetic characteristics

In spring (Apr.-May), the average discharge is 85, 81, and $72 \text{ m}^3 \text{ s}^{-1}$ in 2004-2007, 2008-2014, and 2015-2018, respectively. We thus observe a slight decrease in total freshwater discharge over time. We define the salinity intrusion as the distance from the mouth at which the salinity equals 2 ppt. The corresponding time-averaged values in spring are 81 km, 79 km, and 83 km in 2004-2007, 2008-2014, and 2015-2018, respectively. In spring, the salinity intrusion does not show major changes during the study period 2004-2018. The time- and system-averaged maximum photosynthetic rate P_{\max} in spring is approximately equal in 2004-2007 and 2008-2014, but significantly lower in 2015-2018. The corresponding time-averaged values are 6.59, 6.44, and $4.31 \text{ mg C (mg Chl-a)}^{-1} \text{ h}^{-1}$, respectively. The corresponding time- and system-averaged growth efficiency α are 0.0165, 0.0168, and $0.0188 \text{ mg C (mg Chl-a)}^{-1} \text{ h}^{-1} [\mu\text{mol photons m}^{-2} \text{ s}^{-1}]^{-1}$, respectively. For the monthly averaged data of the discharge, salinity intrusion, P_{\max} , and α covering the full year, we refer the reader to the Supporting Information.

3.2. Evolution of Chl-a studied using model experiments

To quantify the impact of the observed trends presented in the previous section and alterations of other factors affecting phytoplankton growth on the Chl-a concentration, we consider the four model scenarios presented in Section 2.3.

384 **3.2.1. Scenario 1: minimum multi-annual change in calibration parameters required to capture the**
 385 **accumulation of Chl-a in the brackish region in spring**

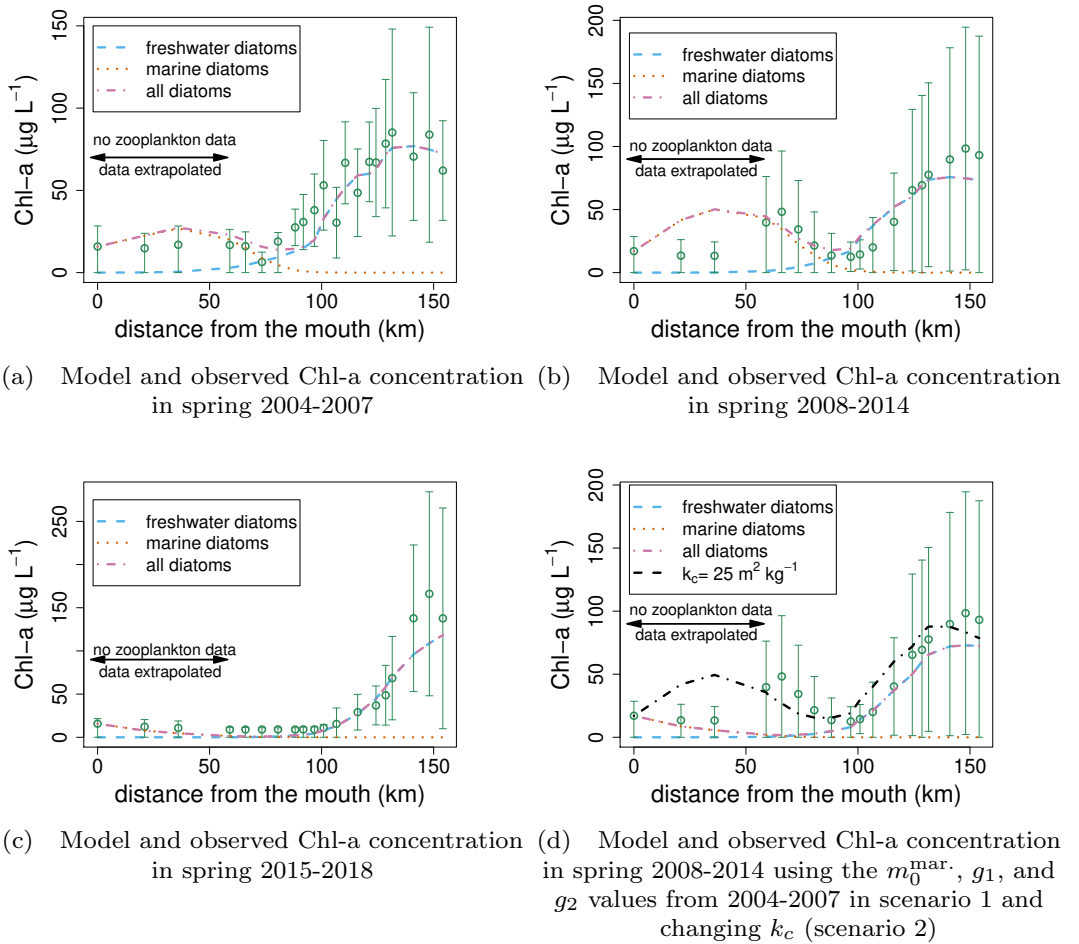


Figure 6: Multi-annual time-averaged Chl-a observations (dots) and depth-averaged model result (dashed line) in spring (Apr.-May) in (a) 2004-2007, (b) 2008-2014, and (c) 2015-2018 (Scenario 1). (d) When we do not consider a multi-annual evolution of parameters $m_0^{\text{mar.}}$, g_1 , and g_2 (Scenario 2), we do not capture the estuary-scale Chl-a distribution in 2008-2014 beyond km 60 (for which we have zooplankton data). A sensitivity analysis shows that by decreasing k_c by a factor ~ 3 ($k_c = 25$ versus $k_c = 78 \text{ m}^2 \text{ kg}^{-1}$), we also obtain accumulation of Chl-a in the brackish region. However, this difference is significantly larger than the variability of k_c that follows from the observations.

386 We calibrate the mortality rate parameters $m_0^{\text{fresh.}}$ and $m_0^{\text{mar.}}$ and grazing parameters g_1 and g_2 to the observed
 387 multi-annual time-averaged Chl-a concentrations for the three periods considered. The corresponding values are listed
 388 in Table 1. In 2004-2007 and 2015-2018, we capture the estuary-scale patterns of Chl-a by keeping the parameters
 389 $m_0^{\text{mar.}}$, g_1 , and g_2 more or less fixed and only changing $m_0^{\text{fresh.}}$ (Figs. 6a and 6c). We require a significantly larger
 390 mortality rate parameter of the freshwater diatoms in 2015-2018 than in 2004-2007 ($m_0^{\text{fresh.}} = 8.30 \times 10^{-6}$ versus
 391 $m_0^{\text{fresh.}} = 1.89 \times 10^{-6} \text{ s}^{-1}$, respectively) to capture the faster decrease of the Chl-a concentrations in the downstream
 392 direction over the years 2004-2018 (depicted by the horizontal arrows in Fig. 3b). Here, it is important to note that
 393 the observed Chl-a values between km 50 and 100 are below the detection limit of $10 \mu\text{g L}^{-1}$ and all modeled Chl-a
 394 concentrations lower than this limit are considered equally good in the calibration. In 2008-2014, we only obtain the
 395 accumulation of Chl-a in the brackish region if we also assume a multi-annual evolution in parameters $m_0^{\text{mar.}}$, g_1 , and

³⁹⁶ g_2 (see Table 1). The calibrated $m_0^{\text{mar.}}$ and g_1 values are ~ 3 and ~ 7 times lower, respectively. If we were to assume
³⁹⁷ no multi-annual evolution of parameters $m_0^{\text{mar.}}$, g_1 , and g_2 after 2007, we would not capture the accumulation of Chl-a
³⁹⁸ in the brackish region (Fig. 6d, red line). To summarize, to capture accumulation of Chl-a in the brackish region in
³⁹⁹ 2008-2014, we require a (significant) multi-annual change in parameters $m_0^{\text{fresh.}}$, $m_0^{\text{mar.}}$, g_1 , and g_2 .

⁴⁰⁰ **3.2.2. Scenario 2: multi-annual change in SPM characteristics required to capture the accumulation of** ⁴⁰¹ **Chl-a in the brackish region in spring**

⁴⁰² Keeping all parameters fixed to their values presented in Table 1 but assuming $m_0^{\text{mar.}}$, g_1 , and g_2 take values from
⁴⁰³ the period 2004-2007 for all periods, a sensitivity analysis shows that variability in μ_{00} , Q , P_{sea} , and QP does not
⁴⁰⁴ result in accumulation of Chl-a in the brackish region in 2008-2014 (for the details, see the Supporting Information).
⁴⁰⁵ We do not focus on $m_0^{\text{fresh.}}$ because marine diatoms dominate the brackish region. Only by decreasing k_c by a factor
⁴⁰⁶ ~ 3 ($k_c = 25$ versus $k_c = 78 \text{ m}^2 \text{ kg}^{-1}$), we obtain accumulation of Chl-a in the brackish region (Fig. 6d, black line).
⁴⁰⁷ This difference is significantly larger than the variability that follows from the observations, which is between ~ 65 and
⁴⁰⁸ $80 \text{ m}^2 \text{ kg}^{-1}$ (for the details, see the Supporting Information). Therefore, a multi-annual change in SPM characteristics
⁴⁰⁹ alone cannot explain the multi-annual evolution in the Chl-a distribution.

⁴¹⁰ **3.2.3. Scenario 3: the individual effect of grazing by zooplankton**

⁴¹¹ In this section, we assume a dominant impact of grazing by zooplankton on the mortality rate (i.e., $m_0^{\text{fresh.}} = 0$
⁴¹² and $m_0^{\text{mar.}} = 0 \text{ s}^{-1}$). Calibration of the grazing parameters g_1 and g_2 to the Chl-a observations in 2004-2007
⁴¹³ and 2015-2018, and the Chl-a observations in the brackish region only in 2008-2014 results in the modeled Chl-a
⁴¹⁴ concentration presented in Fig. 7. Our calibration results in larger grazing parameters because we neglected other
⁴¹⁵ processes contributing to the mortality rate (e.g., salinity stress). The grazing parameters are $g_1 = 2.5 \times 10^{-7}$ and
⁴¹⁶ $g_2 = 0.93 \times 10^{-7} \text{ s}^{-1} \text{ L ind.}^{-1}$, $g_1 = 0.51 \times 10^{-7}$ and $g_2 = 0.71 \times 10^{-7} \text{ s}^{-1} \text{ L ind.}^{-1}$, and $g_1 = 2.5 \times 10^{-7}$ and
⁴¹⁷ $g_2 = 0.93 \times 10^{-7} \text{ s}^{-1} \text{ L ind.}^{-1}$ in 2004-2007, 2008-2014, and 2015-2018, respectively. In 2004-2007 and 2015-2018,
⁴¹⁸ although we detect some local anomalies (for example, the underestimation near km 90 in 2004-2007), the model
⁴¹⁹ captures the Chl-a distribution on the estuary-scale using the same g_1 and g_2 values. In contrast, if we were to choose
⁴²⁰ these calibrated grazing parameter values in 2008-2014, we would obtain a Chl-a distribution very similar to the case
⁴²¹ presented in Fig. 6d (all diatoms) and we would thus not capture the accumulation of Chl-a in the brackish region
⁴²² (not shown). Considering different values for g_1 and g_2 in 2008-2014, we can again model the estuary-scale Chl-a
⁴²³ patterns. Finally, choosing the g_1 and g_2 values corresponding to 2008-2014 in 2015-2018 results in a system-scale
⁴²⁴ overestimation of Chl-a (not shown). To summarize, when only including the effect of grazing by zooplankton, we
⁴²⁵ again require a (significant) multi-annual evolution of g_1 and g_2 to capture the accumulation of Chl-a in the brackish
⁴²⁶ region in spring in 2008-2014.

⁴²⁷ **3.2.4. Scenario 4: neglecting the effect of grazing by zooplankton**

⁴²⁸ In this section, we neglect the impact of grazing by zooplankton to the mortality rate (i.e., $g_1 = 0$ and $g_2 = 0 \text{ s}^{-1}$
⁴²⁹ L ind.^{-1}). We calibrate the mortality rate parameters $m_0^{\text{fresh.}}$ and $m_0^{\text{mar.}}$, while keeping all other parameters fixed to the
⁴³⁰ calibrated values presented in Table 1 (Figs. 7a-7c). The calibration results in larger mortality rate parameters, which is
⁴³¹ due to the absence of grazing pressure. In 2004-2007, we capture the large-scale pattern of the Chl-a distribution using
⁴³² a ~ 70 % larger mortality rate parameter for the marine diatoms ($m_0^{\text{fresh.}} = 3.8 \times 10^{-6}$ versus $m_0^{\text{mar.}} = 6.4 \times 10^{-6} \text{ s}^{-1}$).
⁴³³ In 2008-2014, the model captures the Chl-a distribution beyond km 59 and the local minimum near \sim km 100. This
⁴³⁴ local minimum results from a clear spatial separation between marine and freshwater diatoms that is caused by salinity
⁴³⁵ stress. In Scenario 3, we attribute this minimum to a local increase in mortality rate resulting from the high calanoid
⁴³⁶ abundance in this region. The model overestimates the Chl-a concentration in the marine region at \sim km 21 and 36.
⁴³⁷ The accumulation of Chl-a in the brackish region mainly corresponds to marine diatoms. This accumulation requires
⁴³⁸ a ~ 3 times lower mortality rate parameter for the marine diatoms ($m_0^{\text{fresh.}} = 6.6 \times 10^{-6}$ versus $m_0^{\text{mar.}} = 2.1 \times 10^{-6}$
⁴³⁹ s^{-1}). Upstream from the local minimum at \sim km 100, we mainly have freshwater diatoms. In 2015-2018, we again
⁴⁴⁰ model the Chl-a distribution accurately on the estuary-scale and have a clear spatial separation between freshwater and
⁴⁴¹ marine diatoms. The marine diatoms have a significantly lower mortality rate parameter ($m_0^{\text{fresh.}} = 6.7 \times 10^{-6}$ versus
⁴⁴² $m_0^{\text{mar.}} = 16.6 \times 10^{-6} \text{ s}^{-1}$). In the following, we focus on the multi-annual evolution of the calibration parameters. The
⁴⁴³ mortality rate parameter corresponding to the marine diatoms is equal in 2004-2007 and 2015-2018 ($m_0^{\text{mar.}} = 6.5 \times 10^{-6}$

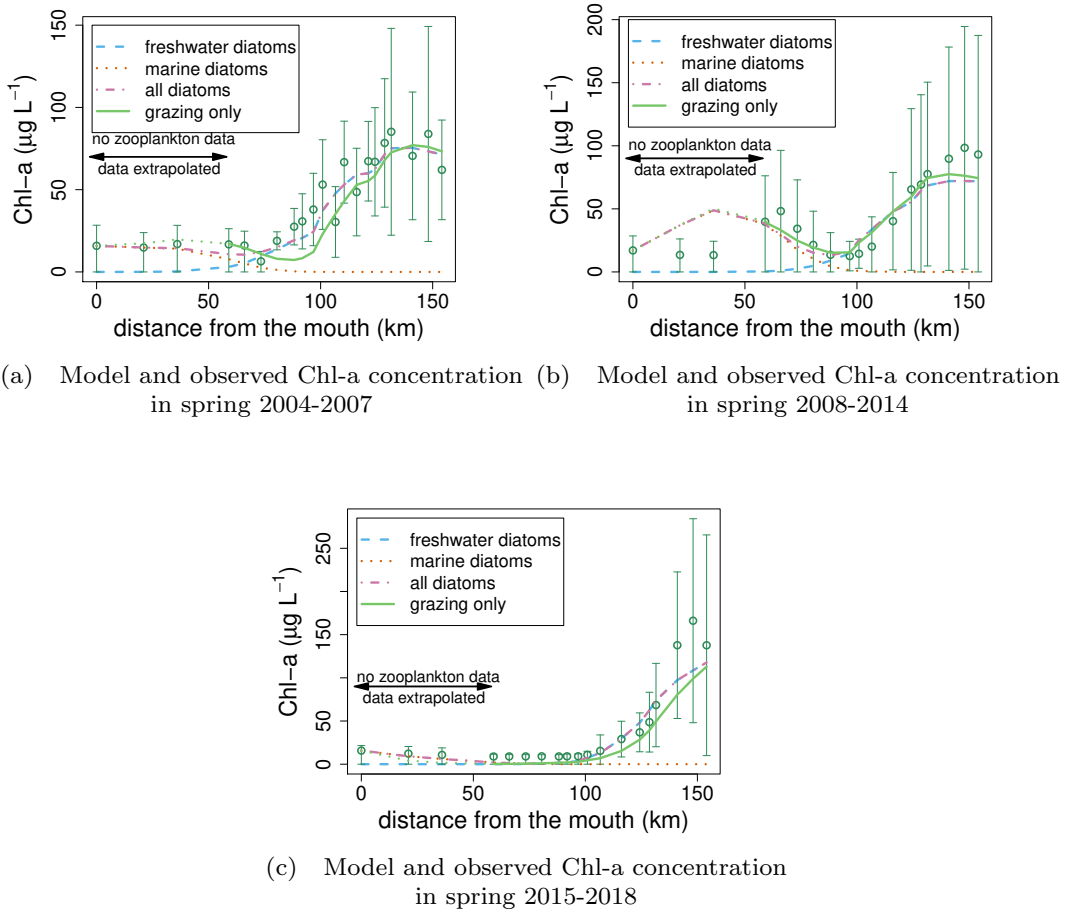


Figure 7: Multi-annual time-averaged Chl-a observations (dots) and depth-averaged model result (dashed/solid line) in spring (Apr.-May) in (a) 2004-2007, (b) 2008-2014, and (c) 2015-2018 assuming a mortality rate exclusively caused by grazing (Scenario 3, denoted by 'grazing only') and neglecting the effect of grazing by zooplankton (Scenario 4, denoted by 'freshwater diatoms', 'marine diatoms', and 'all diatoms').

444 s^{-1}), but significantly lower in 2008-2014 ($m_0^{\text{mar.}} = 2.1 \times 10^{-6} s^{-1}$). As found before, the model also shows a multi-
 445 annual increase of $m_0^{\text{fresh.}}$. For the freshwater diatoms, we have $m_0^{\text{fresh.}} = 3.8 \times 10^{-6} s^{-1}$, $m_0^{\text{fresh.}} = 6.6 \times 10^{-6} s^{-1}$, and
 446 $m_0^{\text{fresh.}} = 16.6 \times 10^{-6} s^{-1}$ in 2004-2007, 2008-2014, and 2015-2018, respectively. To summarize, when excluding the
 447 effect of grazing on the mortality rate, we again require a (significant) multi-annual evolution of $m_0^{\text{fresh.}}$ and $m_0^{\text{mar.}}$ to
 448 capture the accumulation of Chl-a in the brackish region in spring in 2008-2014.

449 4. Discussion

450 4.1. Suggested importance of grazing and phytoplankton community characteristics

451 We studied the appearance and disappearance of accumulation of Chl-a in the brackish region of the Scheldt
 452 estuary in spring in 2008-2014. To this end, we analyzed multi-annual observations of factors affecting phytoplankton
 453 growth and ran various model scenarios. The model approach allowed us to detect which combination of multi-annual
 454 parameter change may result in the multi-annual evolution of the Chl-a concentrations. Our results suggest that we
 455 require a multi-annual shift in phytoplankton mortality rate to capture the appearance and disappearance of Chl-a

456 accumulation in the brackish region and that other parameters (e.g., SPM) alone cannot explain this observed trend of
457 Chl-a.

458 The multi-annual evolution in mortality rate may be attributed to either a change in phytoplankton community
459 characteristics or grazing by zooplankton or a combination. The community characteristics are parameterized by
460 the mortality parameters and salinity stress. It can additionally include changed growth rates related to alterations
461 in nutrient ratios and nutrient forms. In our study, this would also be reflected in changing mortality parameters
462 through processes such as mixotrophy and the excretion of allelopathic compounds or toxins (Glibert et al., 2012).
463 Given the currently available data, further constraining to the exact process(es) that are responsible for the changes in
464 the model parameters is not feasible. However, the potential contribution of nutrient ratios and forms to explain the
465 multi-annual changes in model parameters (m , g) may be a good incentive to collect data of the effect of nutrient ratios
466 on phytoplankton abundance in the Scheldt estuary in the future. We thus found that different changes in processes
467 (including grazing, phytoplankton community composition, and reaction to different nutrient ratios), reflected in
468 various model input parameters, lead to similar model results given the available observations (i.e., equifinality).

469 Although we may not further constrain the relative importance of grazing by zooplankton and phytoplankton
470 community characteristics to the mortality rate, we can compare our calibrated model parameter values to the literature
471 as a first verification of our model results. Our mortality rate (i.e., m) values $\sim 10^{-6} \text{ s}^{-1}$ comply with the value of
472 $\sim 1.1 \times 10^{-6} \text{ s}^{-1}$ presented in Desmit et al. (2005) who studied a real-case in the Scheldt estuary near km 115.
473 Additionally, incubation experiments carried out with adult *Eurytemora affinis* around km 80 in the Scheldt estuary
474 during spring 2013 and 2014 show g values between 1.54×10^{-8} and $2.78 \times 10^{-6} \text{ s}^{-1} \text{ L}$ (Chambord et al., in prep.),
475 overlapping with the modeled values in this study, but also showing large variability. To further constrain which multi-
476 annual change in model parameters may have resulted in the multi-annual change in Chl-a accumulation, additional
477 observations are required.

478 4.2. Model limitations and comparison to literature

479 In this section, we reflect on some of our assumptions and model limitations in context of other literature on the
480 Scheldt estuary.

481 Although our model captures the estuarine-scale patterns of Chl-a, we also see some local mismatches. For
482 example, the model underestimates the Chl-a concentration at \sim km 21 and 36 (Fig. 7b). This may be explained
483 by the existence of a phytoplankton group adapted to specific nutrient ratios or more intermediate salinity, which we,
484 following Naithani et al. (2016), did not consider in the model. As pointed out by Gypens et al. (2013), the presence
485 of euryhaline phytoplankton species may significantly impact the magnitude and distribution of both freshwater and
486 marine phytoplankton. Additionally, in the summer of 2003, the phytoplankton community characteristics showed
487 species with different salinity optima and rather restricted salinity tolerances (Muylaert et al., 2009). We argue that
488 neglecting euryhaline phytoplankton species is acceptable within the scope of this contribution because the model
489 captures the estuarine-scale patterns of Chl-a and adding additional phytoplankton groups would increase equifinality.

490 Another limitation of our modeling approach is that we do not capture all temporal variability of Chl-a (e.g., \sim
491 hours-days) since we solved the equations in equilibrium state and not in a transient manner. We thereby neglected
492 the effect of temporal variability caused by, for example, extreme (weather) events. We argue that this assumption
493 is acceptable because, firstly, the accumulation of phytoplankton in the brackish region covers approximately two
494 months, which is large compared to the time scale of a bloom (\sim 2-3 weeks). Secondly, we observed the accumulation
495 of phytoplankton consistently over seven consecutive years (2008-2014). If the system were to be sensitive to extreme
496 (weather) conditions, we would expect more variability over these seven years.

497 Finally, lateral variations are not present in our observations nor model results. The reason is that, firstly,
498 observations in the lateral dimension are not part of the monitoring programs that we referred to in this contribution.
499 Secondly, following, for example, Gypens et al. (2013) and Naithani et al. (2016), we modeled the width-averaged
500 phytoplankton dynamics only to avoid complex lateral circulation patterns and depth variations. We reason that this
501 suffices for our aim because we focus on estuarine-scale patterns of Chl-a in a well-mixed estuary (Baeyens et al.,
502 1997).

503 To summarize, although a careful assessment of the model assumptions is required, our model is generally
504 applicable to turbid nutrient-rich, tide-dominated estuaries. The approach is particularly useful to constrain parameter
505 ranges, quantify model parameters in more advanced state-of-the-art models, and determine which empirical data is
506 recommended for further research on this topic.

507 5. Conclusions

508 In this contribution, we studied the multi-annual estuary-scale evolution of the spring phytoplankton (cf. Chl-a)
509 distribution in the Scheldt estuary. We focused on the appearance and disappearance of phytoplankton accumulation
510 in the brackish region in spring in 2004-2018.

511 We first analyzed multi-annual in situ observations covering the SPM concentration, zooplankton abundance, and
512 other variables affecting net phytoplankton growth, showing a multi-annual estuary-scale evolution of not only the
513 SPM distribution and zooplankton abundance, but also of the freshwater discharge and phytoplankton photosynthetic
514 characteristics. Next, to detect the multi-annual evolution of these variables that can be linked to the evolution
515 of phytoplankton, we employed a model approach that consisted of an extensive sensitivity study and four model
516 scenarios, and in which the observations were the core. Our model allowed us to significantly constrain which
517 evolution of variables may explain the evolution of phytoplankton; both a multi-annual change in mortality rate and
518 corresponding grazing by zooplankton and phytoplankton community characteristics may have caused the multi-annual
519 estuary-scale evolution of phytoplankton in spring. We were thus able to limit the number of model input parameter
520 choices leading to similar model results.

521 Although our model approach simplifies reality and shows (local) anomalies when comparing phytoplankton
522 model results and observations, it allowed us to quantitatively determine the importance of various factors affecting
523 phytoplankton growth on the estuary scale. This knowledge is important for moving forward using more complex
524 numerically costly models. Our results highlight the importance of insight into the zooplankton dynamics and
525 phytoplankton community characteristics to understand the phytoplankton dynamics in the Scheldt estuary. Before our
526 work, the observed trend change in Chl-a in spring was poorly described and it was unclear whether this trend change
527 is related to changes in physical characteristics (SPM, discharge, temperature) or changes in biological characteristics.
528 In our contribution, we can constrain this to a change in biological characteristics related to phytoplankton mortality
529 that seems to have some correlation with zooplankton grazing and phytoplankton community characteristics. Further
530 research and experimental validation are required to determine the mechanisms that may have caused these multi-
531 annual estuary-scale changes in mortality rate, grazing, and phytoplankton community characteristics.

532 Acknowledgements

533 We thank T. Maris (<https://orcid.org/0000-0002-9819-6771>), De Vlaamse Waterweg NV, and Rijkswa-
534 terstaat for providing all data presented in this paper, F. Azémar (<https://orcid.org/0000-0002-3098-8676>)
535 and C. A. Sossou for their contribution to the zooplankton data set, T. Van Engeland (<https://orcid.org/0000-0002-3590-8831>)
536 for the approval to use the ScheldeData package to generate the illustration of the Scheldt
537 estuary (Fig. 2), S. Jacobs (<https://orcid.org/0000-0003-4831-0844>) for his critical review on the land-inward
538 shift of zooplankton and the connection to the evolution of Chl-a concentration (Fig. 4), H. de Swart (<https://orcid.org/0000-0003-4888-1620>),
539 J. Garnier (<https://orcid.org/0000-0001-9416-9242>), and two anonymous
540 referees for reviewing this manuscript, and H. M. Schuttelaars (<https://orcid.org/0000-0001-8191-6296>) for
541 support, inspiration, and critical review of this work. Author D. M. L. Horemans was an SB PhD fellow at FWO
542 (1S36518N). The data can be accessed on request through <http://www.omes-monitoring.be/en/>.

543 CRediT authorship contribution statement

544 **Dante M. L. Horemans:** Conceptualization, Data curation, Formal analysis, Funding acquisition, Investigation,
545 Methodology, Software, Validation, Visualization, Writing: original draft preparation, Writing: review & editing. **Yoeri**
546 **M. Dijkstra:** Conceptualization, Data curation, Methodology, Software, Supervision, Validation, Writing: review
547 & editing. **Michèle Tackx:** Data curation, Writing: review & editing. **Patrick Meire:** Funding acquisition, Project
548 administration, Resources. **Tom J. S. Cox:** Funding acquisition, Project administration.

549 References

- 550 Alpine, A.E., Cloern, J.E., 1992. Trophic interactions and direct physical effects control phytoplankton biomass and production in an estuary.
551 *Limnology and Oceanography* 37, 946–955. doi:10.4319/lo.1992.37.5.0946.
552 Appeltans, W., 2003. Zooplankton in the Schelde estuary (Belgium/The Netherlands). The distribution of *Eurytemora affinis*: effect of oxygen?
553 *Journal of Plankton Research* 25, 1441–1445. doi:10.1093/plankt/fbg101.

- 554 Arndt, S., Lacroix, G., Gypens, N., Regnier, P., Lancelot, C., 2011. Nutrient dynamics and phytoplankton development along an estuary-coastal
555 zone continuum: A model study. *Journal of Marine Systems* 84, 49–66. doi:10.1016/j.jmarsys.2010.08.005.
- 556 Baeyens, W., Van Eck, B., Lambert, C., Wollast, R., Goeyens, L., 1997. General description of the Scheldt estuary. *Hydrobiologia* 366, 1–14.
557 doi:10.1023/a:1003164009031.
- 558 Billen, G., Garnier, J., 1997. The Phison River plume: Coastal eutrophication in response to changes in land use and water management in the
559 watershed. *Aquatic Microbial Ecology* 13, 3–17. doi:10.3354/ame013003.
- 560 Brion, N., Verbanck, M.A., Bauwens, W., Elskens, M., Chen, M., Servais, P., 2015. Assessing the impacts of wastewater treatment implementation
561 on the water quality of a small urban river over the past 40 years. *Environmental Science and Pollution Research* 22, 12720–12736.
562 doi:10.1007/s11356-015-4493-8.
- 563 Brouwer, R.L., Schramkowski, G.P., Dijkstra, Y.M., Schuttelaars, H.M., 2018. Time Evolution of Estuarine Turbidity Maxima in Well-Mixed,
564 Tidally Dominated Estuaries: The Role of Availability- and Erosion-Limited Conditions. *Journal of Physical Oceanography* 48, 1629–1650.
565 doi:10.1175/JPO-D-17-0183.1.
- 566 Chambord, S., Maris, T., Colas, F., Van Engeland, T., Sossou, A.C., Azémar, F., Le Coz, M., Cox, T., Buisson, L., Souissi, S., Meire, P., Tackx, M.,
567 2016. Mesozooplankton affinities in a recovering freshwater estuary. *Estuarine, Coastal and Shelf Science* 177, 47–59. doi:10.1016/j.ecss.
568 2016.04.016.
- 569 Cira, E.K., Paerl, H.W., Wetz, M.S., 2016. Effects of Nitrogen Availability and Form on Phytoplankton Growth in a Eutrophied Estuary (Neuse
570 River Estuary, NC, USA). *PLOS ONE* 11. doi:10.1371/journal.pone.0160663.
- 571 Cox, T.J., Maris, T., Soetaert, K., Conley, D.J., Van Damme, S., Meire, P., Middelburg, J.J., Vos, M., Struyf, E., 2009. A macro-tidal freshwater
572 ecosystem recovering from hypereutrophication: The Schelde case study. *Biogeosciences* 6, 2935–2948. doi:10.5194/bg-6-2935-2009.
- 573 Cox, T.J.S., Maris, T., Van Engeland, T., Soetaert, K., Meire, P., 2019. Critical transitions in suspended sediment dynamics in a temperate meso-tidal
574 estuary. *Scientific Reports* 9, 12745. doi:10.1038/s41598-019-48978-5.
- 575 Denman, K.L., Pea, M.A., 2002. The response of two coupled one-dimensional mixed layer/planktonic ecosystem models to climate change in the
576 NE subarctic Pacific Ocean. *Deep-Sea Research Part II: Topical Studies in Oceanography* 49, 5739–5757. doi:10.1016/S0967-0645(02)
577 00212-6.
- 578 Desmit, X., Vanderborght, J.P., Regnier, P., Wollast, R., 2005. Control of phytoplankton production by physical forcing in a strongly tidal, well-mixed
579 estuary. *Biogeosciences* 2, 205–218. doi:10.5194/bg-2-205-2005.
- 580 Dijkstra, Y.M., Brouwer, R.L., Schuttelaars, H.M., Schramkowski, G.P., 2017. The iFlow modelling framework v2.4: a modular idealized process-
581 based model for flow and transport in estuaries. *Geoscientific Model Development* 10, 2691–2713. doi:10.5194/gmd-10-2691-2017.
- 582 Dijkstra, Y.M., Chant, R.J., Reinfeldt, J.R., 2019a. Factors Controlling Seasonal Phytoplankton Dynamics in the Delaware River Estuary: an
583 Idealized Model Study. *Estuaries and Coasts* 42, 1839–1857. doi:10.1007/s12237-019-00612-3.
- 584 Dijkstra, Y.M., Schuttelaars, H.M., Schramkowski, G.P., 2019b. Can the Scheldt River Estuary become hyperturbid? A model analysis of suspended
585 sediment concentrations and transport in response to channel deepening. *Ocean Dynamics* 69, 809–827. doi:10.1007/s10236-019-01277-z.
- 586 Dijkstra, Y.M., Schuttelaars, H.M., Schramkowski, G.P., Brouwer, R.L., 2019c. Modelling the Transition to High Sediment Concentrations as a
587 Response to Channel Deepening in the Ems River Estuary. *Journal of Geophysical Research-Oceans* URL: [https://doi.org/10.1029/
588 2018JC014367](https://doi.org/10.1029/2018JC014367), doi:10.1029/2018JC014367.
- 589 Eilers, P.H.C., Peeters, J.C.H., 1988. A Model for the Relationship Between Light-Intensity and the Rate of Photosynthesis in Phytoplankton.
590 *Ecological Modelling* 42, 199–215. doi:10.1016/0304-3800(88)90057-9.
- 591 Eppley, R.W., 1972. Temperature and phytoplankton growth in the sea. *Fish. bull* 70, 1063–1085.
- 592 Filardo, M.J., Dunstan, W.M., 1985. Hydrodynamic control of phytoplankton in low salinity waters of the James River estuary, Virginia, U.S.A.
593 *Estuarine, Coastal and Shelf Science* 21, 653–667. doi:10.1016/0272-7714(85)90064-2.
- 594 Franks, P.J.S., 2009. Planktonic ecosystem models: perplexing parameterizations and a failure to fail. *Journal of Plankton Research* 31, 1299–1306.
595 doi:10.1093/plankt/fbp069.
- 596 Friedrichs, M.A., Dusenberry, J.A., Anderson, L.A., Armstrong, R.A., Chai, F., Christian, J.R., Doney, S.C., Dunne, J., Fujii, M., Hood, R.,
597 McGillicuddy, D.J., Moore, J.K., Schartau, M., Spitz, Y.H., Wiggert, J.D., 2007. Assessment of skill and portability in regional marine
598 biogeochemical models: Role of multiple planktonic groups. *Journal of Geophysical Research: Oceans* 112. doi:10.1029/2006JC003852.
- 599 Friedrichs, M.A., Hood, R.R., Wiggert, J.D., 2006. Ecosystem model complexity versus physical forcing: Quantification of their relative impact with
600 assimilated Arabian Sea data. *Deep-Sea Research Part II: Topical Studies in Oceanography* 53, 576–600. doi:10.1016/j.dsr2.2006.01.026.
- 601 Glibert, P.M., Burkholder, J.A.M., Kana, T.M., 2012. Recent insights about relationships between nutrient availability, forms, and stoichiometry,
602 and the distribution, ecophysiology, and food web effects of pelagic and benthic prochlorococcus species. *Harmful Algae* 14, 231–259.
603 doi:10.1016/J.HAL.2011.10.023.
- 604 Gypens, N., Delhez, E., Vanhoute-Brumier, A., Burton, S., Thieu, V., Passy, P., Liu, Y., Callens, J., Rousseau, V., Lancelot, C., 2013. Modelling
605 phytoplankton succession and nutrient transfer along the Scheldt estuary (Belgium, The Netherlands). *Journal of Marine Systems* 128, 89–105.
606 doi:10.1016/j.jmarsys.2012.10.006.
- 607 Horemans, D.M.L., Dijkstra, Y.M., Schuttelaars, H.M., Meire, P., Cox, T.J.S., 2020a. Unraveling the essential effects of flocculation on large-scale
608 sediment transport patterns in a tide-dominated estuary. *Journal of Physical Oceanography* 50, 1957–1981. doi:10.1175/jpo-d-19-0232.1.
- 609 Horemans, D.M.L., Meire, P., Cox, T.J.S., 2020b. The impact of temporal variability in light-climate on time-averaged primary production and a
610 phytoplankton bloom in a well-mixed estuary. *Ecological Modelling* 436, 109287. doi:10.1016/j.ecolmodel.2020.109287.
- 611 Kromkamp, J., Peene, J., 1995. Possibility of net phytoplankton primary production in the turbid Schelde Estuary (SW Netherlands). *Marine
612 Ecology Progress Series* 121, 249–259. doi:10.3354/meps121249.
- 613 Lancelot, C., Spitz, Y., Gypens, N., Ruddick, K., Becquevort, S., Rousseau, V., Lacroix, G., Billen, G., 2005. Modelling diatom and Phaeocystis
614 blooms and nutrient cycles in the Southern Bight of the North Sea: The MIRO model. *Marine Ecology Progress Series* 289, 63–78.
615 doi:10.3354/meps289063.

- 616 Le Coz, M., Chambord, S., Meire, P., Maris, T., Azémar, F., Ovaert, J., Buffan-Dubau, E., Kromkamp, J.C., Sossou, A.C., Prygiel, J., Spronk, G.,
 617 Lamothe, S., Ouddane, B., Rabodonirina, S., Net, S., Dumoulin, D., Peene, J., Souissi, S., Tackx, M., 2017. Test of some ecological concepts on
 618 the longitudinal distribution of zooplankton along a lowland water course. *Hydrobiologia* 802, 175–198. doi:10.1007/s10750-017-3256-6.
- 619 Lionard, M., Azémar, F., Boulêtreau, S., Muylaert, K., Tackx, M., Vyverman, W., 2005. Grazing by meso- and microzooplankton on phytoplankton
 620 in the upper reaches of the Schelde estuary (Belgium/The Netherlands). *Estuarine, Coastal and Shelf Science* 64, 764–774. doi:10.1016/J.
 621 ECSS.2005.04.011.
- 622 Liu, B., de Swart, H.E., 2015. Impact of river discharge on phytoplankton bloom dynamics in eutrophic estuaries: A model study. *Journal of Marine*
 623 *Systems* 152, 64–74. doi:10.1016/j.jmarsys.2015.07.007.
- 624 Lucas, L.V., Cloern, J.E., Koseff, J.R., Monismith, S.G., Thompson, J.K., 1998. Does the Sverdrup critical depth model explain bloom dynamics
 625 in estuaries? *Journal of Marine Research* 56, 375–415. doi:10.1357/002224098321822357.
- 626 van Maren, D.S., Cronin, K., 2016. Uncertainty in complex three-dimensional sediment transport models: equifinality in a model application of the
 627 Ems Estuary, the Netherlands. *Ocean Dynamics* 66, 1665–1679. doi:10.1007/s10236-016-1000-9.
- 628 Maris, T. and Oosterlee, L., Meire, P., 2013. Onderzoek naar de gevolgen van het Sigmaphan, baggeractiviteiten en havenuitbreiding in de Zeeschelde
 629 op het milieu. Geïntegreerd eindverslag van het onderzoek verricht in 2011. Technical Report Report Ecosystem Management Research Group
 630 ECOBE, 013-R155. University of Antwerp. Antwerp, Belgium. URL: <http://www.vliz.be/imisdocs/publications/82/251782.pdf>.
- 631 Maris, T. and Van Damme, S., Meire, P., 2007. Onderzoek naar de gevolgen van het Sigmaphan, baggeractiviteiten en havenuitbreiding in de
 632 zeeschelde op het milieu. Geïntegreerd eindverslag van het onderzoek verricht in 2006-2007. Technical Report Report Ecosystem Management
 633 Research Group ECOBE, 07-107. University of Antwerp. Antwerp, Belgium. URL: [http://www.vliz.be/imisdocs/publications/](http://www.vliz.be/imisdocs/publications/136054.pdf)
 634 [136054.pdf](http://www.vliz.be/imisdocs/publications/136054.pdf).
- 635 Maris, T. and Van Damme, S., Meire, P., 2009. Onderzoek naar de gevolgen van het Sigmaphan, baggeractiviteiten en havenuitbreiding in de
 636 zeeschelde op het milieu. Geïntegreerd eindverslag van het onderzoek verricht in 2008-2009. Technical Report Report Ecosystem Management
 637 Research Group ECOBE, 010-R124. University of Antwerp. Antwerp, Belgium. URL: [http://www.vliz.be/imisdocs/publications/](http://www.vliz.be/imisdocs/publications/214390.pdf)
 638 [214390.pdf](http://www.vliz.be/imisdocs/publications/214390.pdf).
- 639 Maris, T., Meire, P., 2017. OMES rapport 2016. Onderzoek naar de gevolgen van het Sigmaphan, baggeractiviteiten en havenuitbreiding in de
 640 Zeeschelde op het milieu. Technical Report Report Ecosystem Management Research Group ECOBE, 017-R206. University of Antwerp.
 641 Antwerp, Belgium. URL: www.vliz.be/imisdocs/publications/310259.pdf.
- 642 Meire, P., Ysebaert, T., Van Damme, S., Van den Bergh, E., Maris, T., Struyf, E., 2005. The Scheldt estuary: a description of a changing ecosystem.
 643 *Hydrobiologia* 540, 1–11. doi:10.1007/s10750-005-0896-8.
- 644 Mialet, B., Azémar, F., Maris, T., Sossou, C., Ruiz, P., Lionard, M., Van Damme, S., Lecerc, A., Muylaert, K., Toumi, N., Meire, P., Tackx, M., 2010.
 645 Spatial spring distribution of the copepod *Eurytemora affinis* (Copepoda, Calanoida) in a restoring estuary, the Scheldt (Belgium). *Estuarine,*
 646 *Coastal and Shelf Science* 88, 116–124. doi:10.1016/j.ecss.2010.03.018.
- 647 Mialet, B., Gouzou, J., Azémar, F., Maris, T., Sossou, C., Toumi, N., Van Damme, S., Meire, P., Tackx, M., 2011. Response of zooplankton to
 648 improving water quality in the Scheldt estuary (Belgium). *Estuarine, Coastal and Shelf Science* 93, 47–57. doi:10.1016/j.ecss.2011.03.015.
- 649 Muylaert, K., Sabbe, K., Vyverman, W., 2009. Changes in phytoplankton diversity and community composition along the salinity gradient of the
 650 Schelde estuary (Belgium/The Netherlands). *Estuarine, Coastal and Shelf Science* 82, 335–340. doi:10.1016/j.ecss.2009.01.024.
- 651 Naithani, J., de Brye, B., Buyze, E., Vyverman, W., Legat, V., Deleersnijder, E., 2016. An ecological model for the Scheldt estuary and tidal rivers
 652 ecosystem: spatial and temporal variability of plankton. *Hydrobiologia* 775, 51–67. doi:10.1007/s10750-016-2710-1.
- 653 Perkin, R.G., Lewis, E.L., 1980. The Practical Salinity Scale 1978: Fitting the Data. *IEEE Journal of Oceanic Engineering* 5, 9–16. doi:10.1109/
 654 JOE.1980.1145441.
- 655 Platt, T., Gallegos, C.L., Harrison, W.G., 1980. Photoinhibition of Photosynthesis in Natural Assemblages of Marine-Phytoplankton. *Journal*
 656 *of Marine Research* 38, 687–701. URL: [http://biblioimarpe.imarpe.gob.pe:8080/bitstream/handle/123456789/1357/BOL%](http://biblioimarpe.imarpe.gob.pe:8080/bitstream/handle/123456789/1357/BOL%20EXTR.%20Investigaci%C3%B3n%20...-18.pdf?sequence=1)
 657 [20EXTR.%20Investigaci%C3%B3n%20...-18.pdf?sequence=1](http://biblioimarpe.imarpe.gob.pe:8080/bitstream/handle/123456789/1357/BOL%20EXTR.%20Investigaci%C3%B3n%20...-18.pdf?sequence=1).
- 658 Regnier, P., Wollast, R., Steefel, C.I., 1997. Long-term fluxes of reactive species in macrotidal estuaries: Estimates from a fully transient,
 659 multicomponent reaction-transport model. *Marine Chemistry* 58, 127–145. doi:10.1016/S0304-4203(97)00030-3.
- 660 Rice, E.W., Baird, R.B., Eaton, A.D., editors, 2017. Standard Methods for the Examination of Water and Wastewater. 23rd ed., American Public
 661 Health Association, American Water Works Association, and Water Environment Federation.
- 662 Rijkswaterstaat, 2020. Rijkswaterstaat official website. URL: <https://www.rijkswaterstaat.nl/english/index.aspx>.
- 663 Steele, J.H., Henderson, E.W., 1992. The role of predation in plankton models. *Journal of Plankton Research* 14, 157–172. doi:10.1093/plankt/
 664 14.1.157.
- 665 Sterner, R.W., Elser, J.J., 2017. Ecological stoichiometry, in: *Ecological Stoichiometry*. Princeton university press.
- 666 Sverdrup, H.U., 1953. On Conditions for the Vernal Blooming of Phytoplankton. *ICES Journal of Marine Science* 18, 287–295. doi:10.1093/
 667 icesjms/18.3.287.
- 668 Tilman, D., Kilham, S.S., Kilham, P., 1982. Phytoplankton Community Ecology: The Role of Limiting Nutrients. *Annual Review of Ecology and*
 669 *Systematics* 13, 349–372. doi:10.1146/annurev.es.13.110182.002025.
- 670 Vegter, F., De Visscher, P.R.M., 1984. Phytoplankton primary production in Brackish Lake Grevelingen (SW Netherlands) during 1976-1981.
 671 *Netherlands Journal of Sea Research* 18, 246–259. doi:10.1016/0077-7579(84)90004-8.
- 672 Warner, J.C., Geyer, W.R., Lerczak, J.A., 2005. Numerical modeling of an estuary: A comprehensive skill assessment. *Journal of Geophysical*
 673 *Research: Oceans* 110, 1–13. doi:10.1029/2004JC002691.
- 674 Waterinfo.be, cited 2019. Measurements and predictions of Waterinfo.be [data]. [Available online at <https://www.waterinfo.be/>].
- 675 Winterwerp, J.C., 2002. On the flocculation and settling velocity of estuarine mud. *Continental Shelf Research* 22, 1339–1360. doi:10.1016/
 676 S0278-4343(02)00010-9.
- 677 Winterwerp, J.C., Wang, Z.B., van Braeckel, A., van Holland, G., Kösters, F., 2013. Man-induced regime shifts in small estuaries—II: a comparison
 678 of rivers. *Ocean Dynamics* 63, 1293–1306. doi:10.1007/s10236-013-0663-8.